Materials and Design 56 (2014) 185–192

Contents lists available at ScienceDirect

Materials and Design

journal homepage: www.elsevier.com/locate/matdes

Friction stir welding of dissimilar materials between AA6061 and AA7075 Al alloys effects of process parameters

J.F. Guo *, H.C. Chen, C.N. Sun, G. Bi, Z. Sun, J. Wei

Singapore Institute of Manufacturing Technology (SIMTech), 71 Nanyang Drive, Singapore 638075, Singapore

ARTICLE INFO

Article history:
Received 12 August 2013
Accepted 29 October 2013
Available online 9 November 2013

Keywords:
Dissimilar materials joining
Friction stir welding
Microstructure
Mechanical properties
Grain refinement

ABSTRACT

Dissimilar AA6061 and AA7075 alloy have been friction stir welded with a variety of different process parameters. In particular, the effects of materials position and welding speed on the material flow, microstructure, microhardness distribution and tensile property of the joints were investigated. It was revealed that the material mixing is much more effective when AA6061 alloy was located on the advancing side and multiple vortexes centers formed vertically in the nugget. Three distinct zones with different extents of materials intercalations were identified and the formation mechanism of the three zones was then discussed. Grain refinement was observed in all three layers across the nugget zone with smaller grains in AA7075 Al layers. All the obtained joints fractured in the heat-affected zone on the AA6061 Al side during tensile testing, which corresponds very well to the minimum values in microhardness profiles. It was found that the tensile strength of the dissimilar joints increases with decreasing heat input. The highest joint strength was obtained when welding was conducted with highest welding speed and AA6061 Al plates were fixed on the advancing side. To facilitate the interpretation, the temperature history profiles in the HAZ and at zones close to TMAZ were also measured using thermocouple and simulated using a three-dimensional computational model.

1. Introduction

Joining of dissimilar materials is very attractive for many applications as we can use the more costly one only where necessary. In fact, dissimilar joining could be frequently faced in many scenarios including automotive, aerospace, electronics and shipbuilding industries, where fusion welding simply is not appropriate due to the large difference of physical and chemical properties between the components to be joined [1–3]. Problems including porosity formation, solidification cracking, and chemical reaction may arise during fusion welding of dissimilar materials although sound welds may be obtained in some limited cases with special attentions to the joint design and preparation, process parameters and filler metals [4–6]. In contrast, friction stir welding (FSW) seems to be a very promising technique as it permits welding dissimilar materials in solid-state while avoiding the drawbacks of fusion welding.

Friction stir welding, first invented at TWI in the early nineties [7], is a relatively new welding technique that has demonstrated its great potential in joining materials that are traditionally considered to be unweldable or difficult to weld. As a variant process of friction welding, it provides the opportunity of welding components with relatively flat geometry at high productivity. FSW is most suitable for welding light metal alloys, Al-based metal matrix composites (MMCs), and dissimilar metals [8,9]. The FSW of light metals has been extensively studied [8] and the FSW of MMCs and/or dissimilar monolithic metals/alloys has also become an important research topic in recent years [1,3]. High quality FSW joints have been obtained between different metals/alloys, MMCs and monolithic alloys [1–3,10–15]. Among these studies, FSW of dissimilar materials between Al alloys has been focused by many researchers and engineers from a variety of industries [1,3,16–20]. It was reported that the temperatures are higher on the advancing side when welding similar materials [8,21]. It is reasonable to believe that the location of the materials in FSW of dissimilar alloys could lead to more severe temperature asymmetry. This asymmetry in temperature, stress and materials flow between the advancing and retreating sides could significantly affect the dissimilar joint quality and properties, which mainly depends on the properties of the two materials and the welding parameters such as tool rotation speed, travel speed and positions of the materials. It was reported that only a portion of material transported from the leading edge undergoes chaotic flow and sound joints without defects can only be obtained when the weld interface is on the advancing side [16]. Better materials mixing can be achieved when using high rotation speeds in the compromise of reduced surface integrity [17,18]. Park et al. [22] and Aval et al. [23]

* Corresponding author. Tel.: +65 6793 2251; fax: +65 6791 6377.
E-mail address: jfguo@simtech.a-star.edu.sg (J.F. Guo).

0261-3069/$ - see front matter © 2013 Elsevier Ltd. All rights reserved.
http://dx.doi.org/10.1016/j.matdes.2013.10.082

revealed that more efficient materials mixing was obtained when the softer AA5xxx aluminum alloy was in the advancing side and the harder AA6xxx aluminum alloy was in the retreating side. Slightly higher transverse tensile strengths of joints were obtained with soft AA5xxx Al alloy on the advancing side [22]. However, the longitudinal tensile strengths (parallel to FSW direction) of joints produced with soft AA5xxx Al alloy on the advancing side showed slightly lower values than the opposite conditions [22]. In another study on FSW of AA6061 and A356 Al alloys, Lee et al. [24] showed that higher longitudinal tensile properties of the weld (parallel to FSW direction) were acquired when a relatively softer material was fixed at the advancing side because the dominant material in the weld zone mainly came from the harder retreating side. It seems the effect of relative position of materials is closely related to the materials pair, no simple prediction can be made before investigation. Sundaram et al. [20] investigated the effects of various process parameters including tool pin profile, tool rotational speed, and welding speed on mechanical properties of the dissimilar joints between AA2024 and AA5083 Al alloys. They reported that dissimilar joints fabricated using tapered hexagon tool pin profile have the highest tensile strength and tensile elongation, whereas the straight cylinder tool pin profile have the lowest tensile strength and tensile elongation [20]. However, the increase in the tool rotational speed or welding speed led to increase in tensile strength initially and then decrease after reaching a maximum value.

It is clear that many progresses have been made in FSW of dissimilar materials but it has to be understood that study on this topic is far from enough and still in the feasibility stage. Up to now, systematic study on FSW of dissimilar materials between AA6xxx and AA7xxx series Al alloys has never been reported to the best of authors' knowledge [25]. AA6xxx and AA7xxx Al alloys are two series of the most widely used structural materials in automotive, rail transportation and aerospace industries. Therefore, the present study using AA6061 and AA7075 Al alloys as the base materials aims to investigate the effects of various process parameters such as welding speed, positions of materials and the resulted heat input on the materials flow, microstructures and mechanical properties of the dissimilar joints.

2. Experimental procedures

The base materials used in the study are rolled plates of AA6061 and AA7075 Al alloy (both are 6.3 mm thick) in T6 temper condition. The chemical compositions of these two alloys are listed in Table 1. All plates were cut before welding into dimensions measuring 300 mm long and 50 mm wide (rolling direction). They were carefully degreased with acetone and dried in air. Butt joints of these plates were then produced along the longitudinal direction using a friction stir welding robot which is capable of generating 12 kN maximum downward force. The welding tool has a shoulder with 15 mm diameter and a threaded conical probe with three flats and 5 mm diameter at probe base. The relative positions of both alloys were varied to investigate its effects on the materials flow and heat input. Three welding/travel speeds were used at a constant tool rotation speed of 1200 rpm. The detailed welding parameters are listed in Table 2.

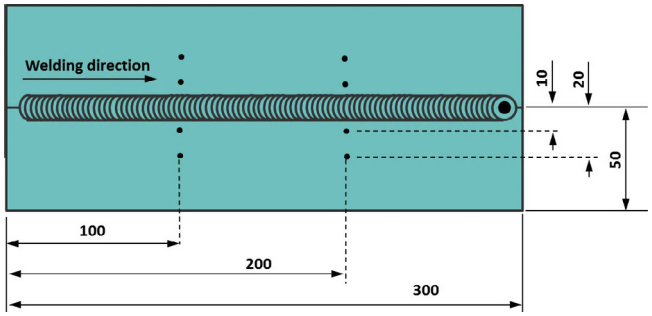

Fig. 1. Schematic illustration showing thermocouple locations during temperature measurements.

The temperature profiles in the heat-affected zones (HAZ) were in situ measured using K-type thermocouples with a 0.25 mm diameter wire. As shown in Fig. 1, four holes (black points) with 2.3 mm diameter were drilled to a depth of 3 mm on each plate. Thermocouples were fixed into the holes with short bars of 1.6 mm diameter 5356 Al filler wire. The filler wires were then mechanically punched to improve the contact between the thermocouples and the workpiece. The temperature history profiles at these locations were recorded at 0.5 s sampling interval using a digital data logger with eight channels. The temperature history profiles in the nugget or zones very close to thermo-mechanically affected zones (TMAZ) were simulated due to the high temperature gradient in these zones and the difficulties in accurately positioning thermocouples. A transient thermal analysis was carried out by using commercial finite element software, ANSYS. In this thermal analysis, the three-dimensional thermal solid element type, SOLID 70, was chosen for the model. In total, the model included 38,505 nodes and 30,000 elements. Temperature-dependent

Table 1
Chemical composition of AA6061 and AA7075 alloys (wt.%) [26].

Alloy	Zn	Mg	Cu	Mn	Si	Fe	Ti	Cr	Al
AA6061	0.25 max	0.8–1.2	0.15–0.4	0.15 max	0.4–0.8	0.7 max	0.15 max	0.04–0.35	Bal.
AA7075	5.1–6.1	2.1–2.9	1.2–2.0	0.3 max	0.4 max	0.5 max	0.2 max	0.18–0.28	Bal.

Table 2
Main FSW parameters used in the study.

Conditions	Materials*	Rotation speed (rpm)	Travel speed (mm/s)	Downward force (kN)	Tilt angle (°)
D1	7075–6061	1200	2	6.6	2.5
D2	7075–6061	1200	3	6.1	2.5
D3	7075–6061	1200	5	7.0	2.5
D4	6061–7075	1200	3	6.0	2.5
D5	6061–7075	1200	5	6.7	2.5

* The materials on the left were located on advancing side during FSW.

material properties of both Al alloys [26], such as thermal conductivity and density were considered in the model.

The welded samples were transversely sectioned and polished using conventional mechanical polishing method. Micro-etching was carried out using Keller's reagent for 20–150 s at ambient temperature to reveal the grain structures of the welds. Microstructural characterization was performed using an optical microscope (OM) and a scanning electron microscope (SEM) equipped with an energy dispersive spectrometry (EDS). The Vickers hardness was also measured across the centre of each joint with 100 gf loading at intervals of about 1 mm. Tensile testing was conducted according to the ASTM E8-04 standard at a test speed of 1 mm min^{-1}. Rectangular flat samples with a 50 mm gauge length and a 12.5 mm width in the reduced section were used.

3. Results and discussions

3.1. Temperature profiles

Friction stir welding is basically a thermo-mechanical process where the materials experience a thermal cycle and mechanical mixing simultaneously. It is well established that the temperature history determines the microstructure evolution during FSW [27,28]. For heat treatable Al alloys, in particular, the local thermal hysteresis could strongly influence the distribution of precipitates and make them coarsen, dissolve and re-precipitate. However, due to the high temperature gradient in the regions close to nugget zone and the difficulties in accurately positioning thermocouples, it is very difficult to measure the temperature profile during FSW in the nugget, TMAZ or locations very close to TMAZ where usually the joints failed during tensile testing. Therefore, only the temperature history profile in HAZ was measured and a computational model proposed by Riahi et al. [29] was used to simulate the temperature profiles in these zones. In this model, the local heat (Q) generated by friction between the tool and the surface of welding materials was applied as in the following equation:

$$Q = \frac{4\pi^2}{3}\mu N p(r_S^3 + 3r_P^2 h) \quad (1)$$

where μ is the friction coefficient between welding tool and Al plates, N is tool rotation speed (1200 rpm), p is local pressure applied by welding tool on the top surface of welding materials (N), r_S is shoulder radius (7.5 mm), r_P is pin radius (2.5 mm) and h is the pin length (6.1 mm).

The Al plates used in the study are 300 mm long, 50 mm wide and 6.3 mm thick. Based on the fixture design and lab environment (23 °C), a heat flux of 350 W/m^2 K from both top and bottom surfaces were assumed while a heat flux of 35 W/m^2 K was considered for side surfaces.

Fig. 2 shows the temperature history profiles obtained from both experiments and simulation at 10 mm away from the joint line on AA6061 Al side for conditions D5. All simulated temperature profiles shown below are calculated at 3 mm from the top surface of Al plates since the ones measured by thermocouples are obtained from the same locations. As seen in Fig. 2, a very close match between the simulated and experimentally measured temperature profiles are observed, which indicates the two-dimensional model built can be used to effectively predict the thermal cycles experiences in other zones where the temperature history profile is difficult/impossible to measure accurately. It was reported that the temperature profile has an asymmetric distribution during FSW [21], especially in welding of dissimilar materials because the materials on advancing and retreating sides have different flow patterns and the two alloys have very different flow stress. The relative position of AA6061 and AA7075 alloys would

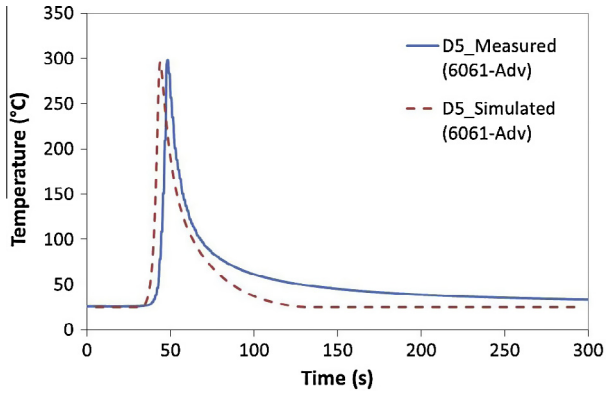

Fig. 2. Measured and simulated temperature history profiles at 10 mm away from the joint line on AA6061 Al side for condition D5.

definitely influence the thermal profile experienced by the materials across the joint. Thus, the temperature history profiles at 8 mm away from the joint line on AA6061 side were simulated for several typical welding conditions and are illustrated in Fig. 3. The 8 mm distance is selected because all joints failed approximately at this location on AA6061 side as will be discussed later in the article. As shown in Fig. 3, at a constant tool rotation speed, much higher peak temperature is obtained at 2 mm/s travel speed compared to that of 5 mm/s travel speed, which can be readily understood because the total friction heat generated during FSW is inversely proportional to the travel speed. At the same rotation and travel speed, slightly higher peak temperature in AA6061 is obtained when AA7075 Al was located on the advancing side. This is due to that the material transport is more intense on the advancing side and AA7075 alloy has much higher flow stress/yield strength than AA6061 alloy does [30].

3.2. Materials flow & microstructure

Fig. 4 shows macro-views of the cross sections of the friction stir welded joints produced under different conditions. The AA6061 alloy features as darker colors, while AA7075 alloy features as light colors because of their different etching response to the Keller's reagent. It is evident that sound joints of AA6061–AA7075 Al alloys were achieved under all the investigated welding conditions. The material mixing seems to be much more effective when AA6061 alloy was located on the advancing side, especially with higher welding speed as seen in Fig. 4b and d. This is mainly because the higher flow stress of harder AA7075 alloy [30], when located on the advancing side, makes it very difficult for AA6061

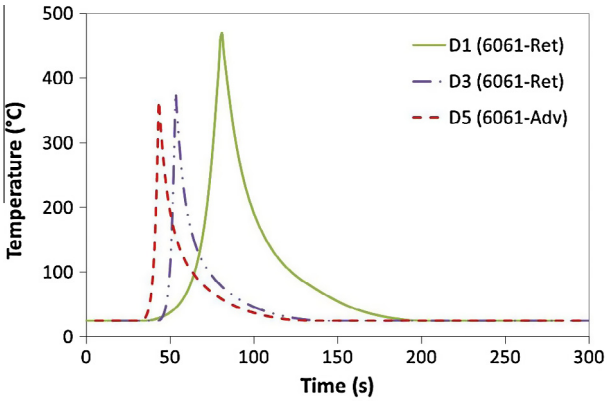

Fig. 3. Simulated temperature history profiles at 8 mm away from the joint line.

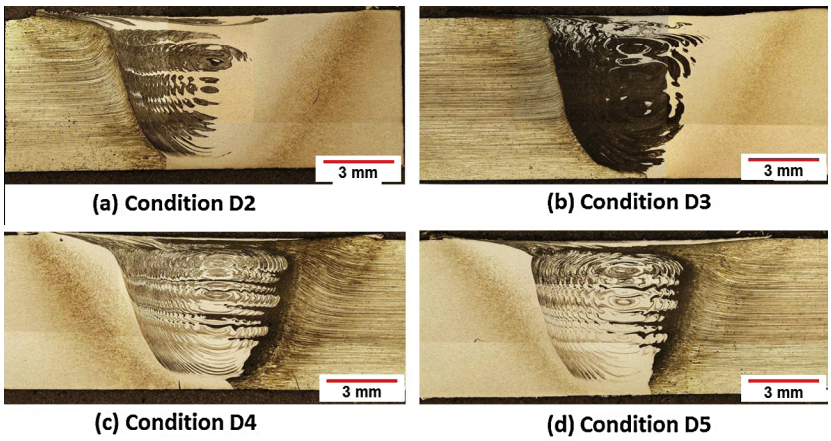

Fig. 4. Macro-views of the cross sections of joints produced under different conditions.

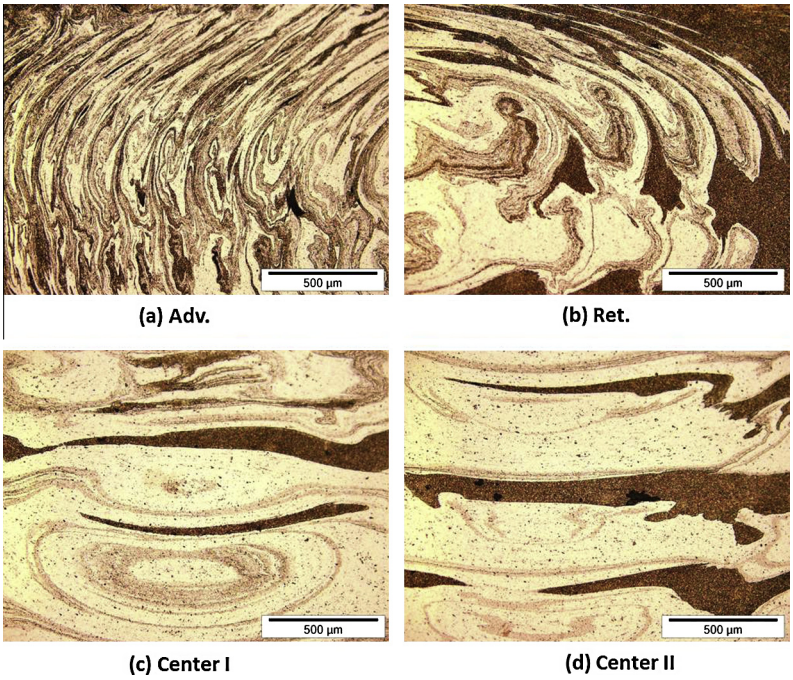

Fig. 5. Images show the complex materials flow patterns (onion rings) on the top advancing and retreating sides: (a and b), and the multiple vortexes in the nugget center: (c and d).

alloy to penetrate into the nugget. In FSW, the materials on retreating side are much less intensely transported around the tool before deposited in the wake of the weld when compared with the ones on advancing side. This is in accordance with the results obtained by Park et al. [22] in FSW of dissimilar AA5051-H32 and AA6061-T6 alloys. They concluded that the materials were more properly mixed when the AA5052-H32 aluminum alloy was in the advancing side than the case of the AA6061-T6 aluminum alloy in the advancing side.

As shown in Fig. 4, onion ring typically seen in FSW was clearly observed in all the joints thank to the different etching responses of the two alloys. It is interesting to notice that a series of vortex centers could be seen vertically in the nugget center especially when the AA6061 alloy was located on the advancing side. The multiple vortexes feature observed in the present study is quite unique since the onion ring layers reported in literature usually belong to only one single vortex center [22,25,31]. Such multiple vortexes compilation has never been reported before to the best of authors' knowledge. The formation mechanism of the multiple vortexes is believed to be related to both of the flats numbers and threads pitch of the tool. The complex materials flow patterns (onion rings) on the top advancing and retreating sides, and the multiple vortexes in the nugget center are illustrated in Fig. 5. Three distinct sub-layers can be observed in the onion rings of the dissimilar welds of AA6061–AA7075 Al alloys. These sub-layers were then further identified as: (a) 6061 alloy sub-layer (spectrum 1), (b) AA7075 alloy sub-layer (spectrum 2), and (c) mixed sub-layer of the two alloys (spectrum 3) by EDS under SEM (Fig. 6). The formations of AA6061 and AA7075 alloy sub-layers are quite straight forward; while the formation of the mixed sub-layer could be attributed to that the plasticized materials contained in the spaces adjacent to the flats may have experienced intense extrusion turbulences and have enough time to be well mixed before finally deposited to the wake of the weld. The thicknesses of these onion ring sub-layers were measured at around 30–100 μm, which are much smaller compared to the

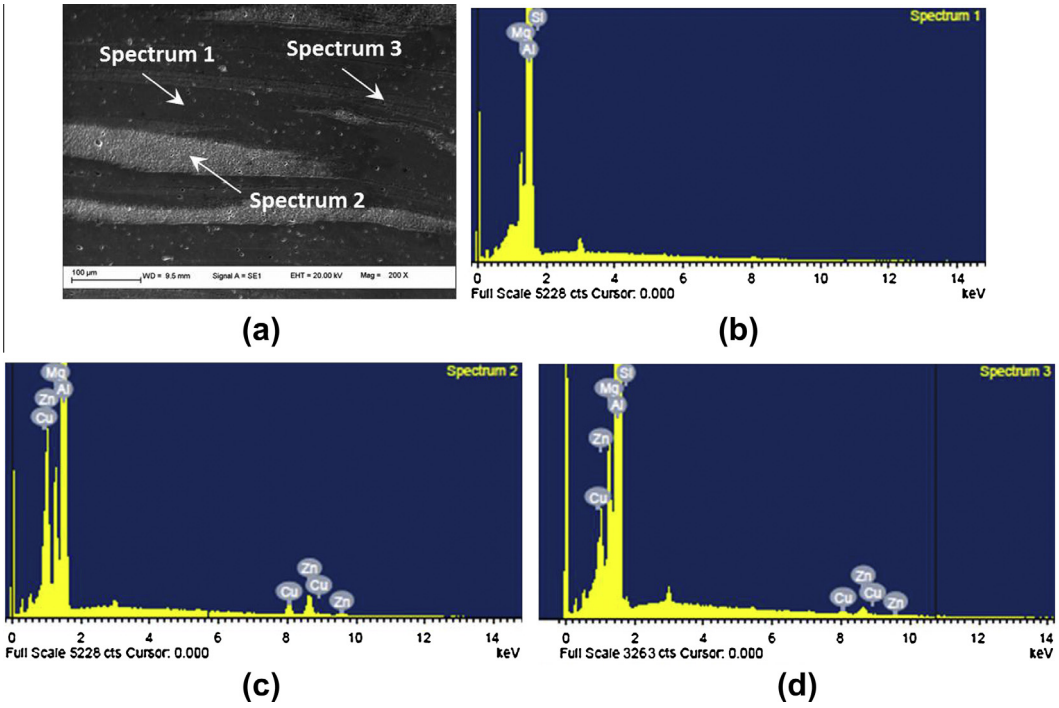

Fig. 6. SEM image and EDS spectrums showing the chemical compositions of the three distinct layers formed in FSW.

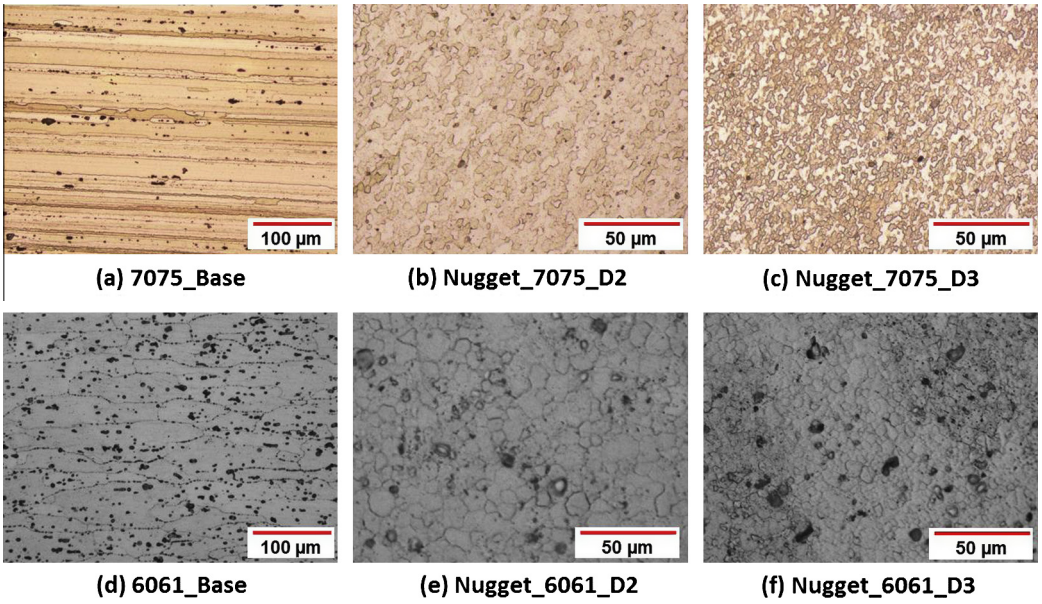

Fig. 7. Optical micrographs showing the grain structures of different alloy sub-layers in the nugget zones of the dissimilar welds and the two base metals.

advance per revolution (100–250 μm) defined as traveling distance of the welding tool per revolution [8]. The much thinner onion ring sub-layers are resulted from that three materials flow waves instead of one have formed during FSW because the tool used in the study has a probe with three flats. Thus, the thicknesses of the onion ring sub-layers are roughly one-third of the advance per revolution.

It is evident that use of dissimilar alloys/materials can be a very effective alternative method to investigate the material flow behavior during FSW. Other methods including inserted copper foil, plated surfaces, and composite markers have been used to study the material flow during FSW [8]. However, those methods only reveal the material flow at one location in the weld. In contrast, the use of dissimilar materials may illustrate the material flow pattern across the whole weld. Nonetheless, the material flow pattern in dissimilar materials joining might be slightly different from that in FSW of similar materials. The above results also indicate that use of FSW tools with multiple flats and threads can be an effective way to achieve seamless bonding during dissimilar materials joining. However, it might be difficult to add such features for tools when joining material pairs involving hard alloys such as steels and super nickel alloys.

Fig. 7 shows the grain structures of different alloy sub-layers in the nugget zones of the dissimilar welds and the two base metals.

Obviously, both AA6061 and AA7075 alloys have experienced dynamic recrystallization. For AA7075 alloy (Fig. 7a–c), the grain structure has been refined from large mm-scale elongated ones to very fine equiaxed ones with less than 6 μm equivalent diameters. The grain size decreased from ~6 μm to ~3 μm when the welding speed increased from 3 mm/s to 5 mm/s. This can be attributed to that slow welding speed resulted in more heat input and longer time of grain growth for the materials in the nugget zones. As shown in Fig. 3, the time span above 200 °C at 2 mm/s is much longer than at 5 mm/s. For AA6061 alloy, the equiaxed grain structure has been refined from around 50 μm to less than 10 μm. Similar as in AA7075 sub-layer, the grain size decreased from ~10 μm to ~5 μm when the welding speed increased from 3 mm/s to 5 mm/s. It has to be noted that the grain size of AA7075 alloy sub-layer is much smaller than that of AA6061 sub-layer in the same weld (Fig. 7b vs. Fig. 7e, Fig. 7c vs. Fig. 7f). The grain size difference was also noted by Srinivasan et al. in a corrosion study on FSW of dissimilar AA7075 and AA6056 alloys [25]. They attributed this difference to the smaller initial grain size of the AA7075 alloy used in their study. However, the grain size difference cannot be explained by their initial grain sizes in the present study since the AA7075 alloy has much larger initial grain size. At such micro-scale, the temperature history at adjacent AA6061 and AA7075 sub-layers should be almost identical. Therefore, such difference is probably due to that AA7075 alloy has much higher alloying elements content than AA6061 alloy does (see Table 1: ~2% vs. ~10%). All second phase particles and intermetallics could provide much more nucleation sites and retard grain growth during recrystallization process, and thus result in finer grain structure. It was reported that second phase particles could provide nuclei during annealing and recrystallization processes [32]. In 7xxx series of Al alloys, zirconium or chromium is added as grain refiner and to retard recrystallization during heat treatment. Thus, all second phase particle in AA7075 alloy including η-$MgZn_2$ precipitates, Al_3Zr dispersoids and Al–Cu–Fe constituent phase particles will provide nucleation sites (larger than 0.5 μm) [33] and pinning effect for recrystallization. In contrast, the content of such second phase particles is much lower in AA6061 alloy compared to that in AA7075 alloy. Detailed discussion on the particle-stimulated nucleation and particle pinning effect is beyond the scope of the present study and can be found elsewhere in literature [33–36].

3.3. Microhardness

Fig. 8 shows the Vicker's microhardness profiles of the cross-section of the dissimilar joints produced under different conditions (D2–D5). In general, both AA6061 and AA7075 alloys have exhibited certain microhardness decrease in the weld compared to their corresponding base metals (both materials are in T6 temper condition). This is mainly because of the coarsening, dissolution and reprecipitation of strengthening precipitates caused by FSW thermal cycle [27,37] although grain structure refinement may also have some minor contributions. In the HAZ, the slightly lower hardness is due to the disappearance of Guinier–Preston (G.P.) zones and coarsening of strengthening precipitates, which is similar to an over-ageing process. In the TMAZ, more severe coarsening and possibly complete dissolution of precipitates occurred due to a similar effect of the solution treatment. In the nugget, some reprecipitation after complete dissolution may have taken place since the material experienced higher temperature in this region. The transition of microhardness in the nugget from AA6061 to AA7075 is more gradual (conditions D2, D4 and D5) when AA6061 alloy was located on the advancing side or lower welding speed is used. This indicates again more effective material mixing is obtained under these welding conditions (Fig. 4a, c and d). In all the cases, as

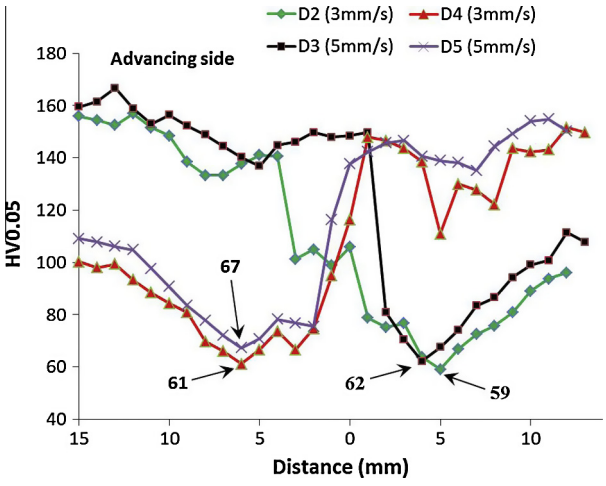

Fig. 8. Vicker's microhardness profiles of the cross-section of dissimilar joints.

the arrows marked in Fig. 8, the hardness minima are observed in the HAZ on the AA6061 side regardless of the relative materials position or the applied process parameters. In fact, all joints failed on the AA6061 side in HAZ regions very close to the TMAZ in tensile testing, where the minimum hardness is located. As described in the previous part (Fig. 3), the peak temperatures at 8 mm away from the joint line (approximately where the hardness minimum is located) reached temperatures higher than 365 °C, which are still lower than the solution heat treatment temperature of AA6061 alloy (530 °C) [38]. The decrease of microhardness in HAZ is due to the disappearance of G.P. zones and coarsening of strengthening precipitates. Thus, less severe precipitate coarsening could occur in the HAZ of the joints produced with lower heat input and hence the hardness profile of the joints produced with the lowest heat input (condition D5) has the highest minimum value as illustrated in Fig. 8.

3.4. Tensile properties

Table 3 shows the tensile properties of the base AA6061 alloy and the dissimilar joints between AA6061and AA7075 alloys. Only the tensile properties of AA6061 alloy are shown in the table because all joints failed on the AA6061 side at positions in HAZ regions where the hardness minima are located. As reported previously in dissimilar FSW of other Al alloys, the friction stir welded joints usually fractured at locations in HAZ on the weaker material side [18,31,39]. However, those investigations did not study the effect of material position on the tensile properties. The failure locations in HAZ also indicate seamless bonding has been achieved between dissimilar AA6061and AA7075 alloys under all investigated welding conditions. As shown in Table 3, all the joints exhibit very good tensile properties with ultimate tensile strength (UTS) higher than 215 MPa and elongation higher than 6%. The highest UTS value is 32% higher than required for FSW of AA6061 alloy at T6 condition in the AWS standard (186 MPa): AWS D17.3/D17.3M:200X [40]. The UTS increases with the increase of welding speed when the location of AA6061/AA7075 alloy is fixed. At a constant welding speed, the UTS are slightly higher when AA6061 alloy was located on the advancing side. The increases of UTS are mainly because FSW at higher welding speed or with AA6061 on the advancing side induced less heat input and thus less severe precipitate coarsening in the HAZ. As illustrated in Fig. 3, the peak temperature at 8 mm away from the joint line decreases from 469 °C to 378 °C with the increase of welding speed from 2 mm/s to 5 mm/s when the AA6061 alloy is fixed on the retreating side. At the same

Table 3
Tensile properties of the dissimilar joints between AA6061and AA7075 alloys.

Conditions	Material on Adv. side	UTS (MPa)	YS (MPa)	ε (%)	Joint efficiency*	Failure location
6061_T6	–	310	276	12	–	–
D1	7075	215 ± 2	160 ± 5	7 ± 1	69	HAZ_6061
D2	7075	221 ± 4	152 ± 3	7 ± 0	71	HAZ_6061
D3	7075	235 ± 3	168 ± 3	6 ± 1	76	HAZ_6061
D4	6061	228 ± 2	159 ± 3	8 ± 1	74	HAZ_6061
D5	6061	245 ± 3	177 ± 6	6 ± 1	79	HAZ_6061

* Joint efficiency defined as the ratio of the UTS of the joint and the base metal at T6 condition.

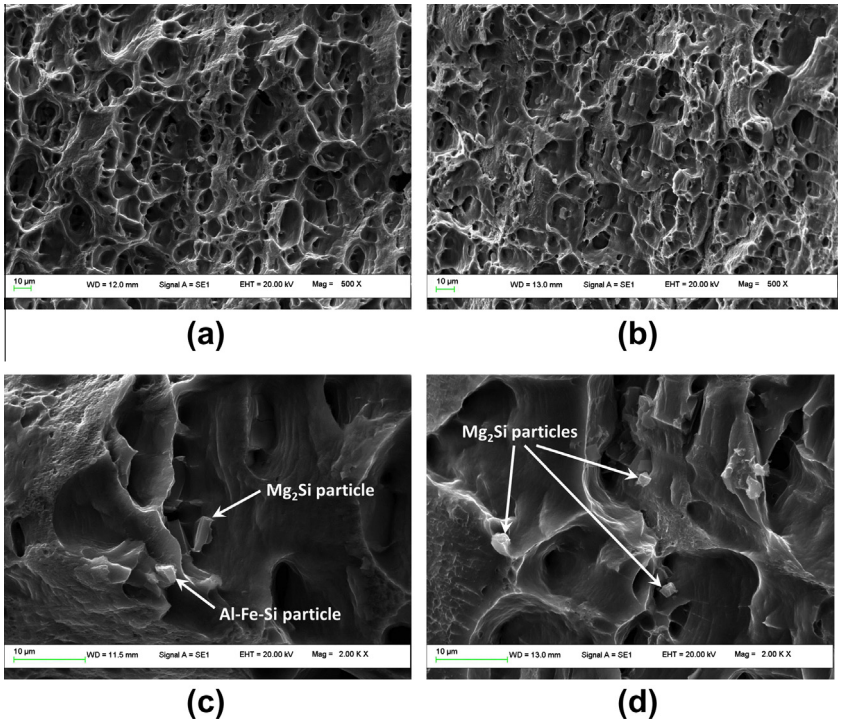

Fig. 9. Fractured surfaces of the tensile tested specimens under SEM for conditions D2 and D5. (a and c): condition D1, (b and d): condition D5.

welding speed at 5 mm/s, the peak temperature decreases slightly from 378 °C to 365 °C when the location of AA6061 alloy was changed from the advancing side to the retreating side. A comparison of the tensile data and the microhardness profiles reveals the tendency of UTS corresponds very well with the tendency of hardness minima, which demonstrates the precipitate evolution caused by FSW thermal cycle determines both the microhardness distribution and tensile property of the joints.

3.5. Fractured surfaces

Fig. 9 shows the fractured surfaces of the tensile tested specimens under SEM for conditions D1 and D5. These two conditions were selected for fractographic analysis because heat input is the main factor determining the tensile properties of joints and the difference of heat input between these two conditions is the most marginal. As seen in Fig. 9a and b, the fractured surfaces are characterized as a large amount of equiaxed dimples with different size. Compared to condition D1, the fractured surface of the joints produced under condition D5 shows shallower dimples. As we know, in such dimple rupture mode, overload is the principal cause of fracture and the failure is governed by coalescence of microvoids. The microvoids may nucleate at regions adjacent to second phase particles, inclusions, grain boundaries, and dislocation pile-ups. Consequently, the microvoids grow, coalesce, and eventually form a continuous fracture surface as the strain increases during tensile testing [41]. Therefore, the reason for the shallower dimples in condition D5 is probably because more severe precipitate coarsening occurred during FSW and thus less closely spaced β-Mg_2Si phase particles has formed in the HAZ of the joints produced under condition D1. Second phase particles including incoherent β-Mg_2Si phase and various Al–Fe–Si intermetallics in AA6061 alloy could effectively provide nucleation sites for microvoids during fracture process. Fig. 9c and d illustrate some examples of such nucleation sites at the bottom of dimples or at the top of ridges. However, quantitative measurement of the amount of such second phase particles is unrealistic since most of the particles are usually hidden at the bottom of the dimples and have similar color as the surrounding Al matrix on fractured surfaces under SEM.

4. Conclusions

Dissimilar AA6061 and AA7075 alloys have been friction stir welded with a variety of different process parameters. At a constant tool rotation speed of 1200 rpm, the effects of materials position and welding speed on materials flow, microstructures, microhardness distributions and tensile properties of the joints

were investigated. Based on the above results and discussion, the following conclusions can be drawn accordingly.

(1) The material mixing is much more effective when AA6061 alloy was located on the advancing side and multiple vortexes centers formed vertically in the nugget center.
(2) The onion ring observed in dissimilar welds of AA6061–AA7075 Al alloys consist of three distinct sub-layers: (a) AA6061 alloy sub-layer, (b) AA7075 alloy sub-layer, and (c) mixed sub-layer of the two alloys. The thicknesses of these onion ring sub-layers were measured at around 30–100 μm which is roughly one-third of the advance per revolution.
(3) Both AA6061 and AA7075 alloys have experienced dynamic recrystallization and the grain size in both alloys decreases significantly with the increase of welding speed. The grain size of AA7075 alloy sub-layer is much smaller than that of AA6061 sub-layer in the same weld.
(4) Both AA6061 and AA7075 alloys have exhibited certain microhardness decrease in the weld compared to their corresponding base metals (both materials are in T6 temper condition). The minimum hardness values are observed in the HAZ on the AA6061 side regardless of the relative materials position or the applied process parameters. The hardness profile of the joints produced with the lowest heat input (condition D5) has the highest minimum value.
(5) All the joints failed at positions in HAZ on the AA6061 side where the minimum hardness is located and exhibited very good tensile strengths and ductility. The UTS of joints increases with the decrease of heat input induced by friction and corresponds very well to the minima in the microhardness profiles. The highest UTS achieved in condition D5 reached 245 MPa which is 32% higher than required in the AWS standard on FSW.
(6) The fractured surfaces of tensile tested specimens are characterized as a large amount of equiaxed dimples with different size. Shallower dimples were observed in the fractured surface of the joints produced under lower heat input. Second phase particles including incoherent β-Mg_2Si and various Al–Fe–Si intermetallics could effectively provide nucleation sites for microvoids during fracture process.

References

[1] DebRoy T, Bhadeshia H. Friction stir welding of dissimilar alloys – a perspective. Sci Technol Weld Joining 2010;15:266–70.
[2] Guo J, Gougeon P, Chen X-G. Microstructure evolution and mechanical properties of dissimilar friction stir welded joints between AA1100-B_4C MMC and AA6063 alloy. Mater Sci Eng A 2012;553:149–56.
[3] Murr LE. A review of FSW research on dissimilar metal and alloy systems. J Mater Eng Perform 2010;19:1071–89.
[4] Ellis MBD. Joining of aluminium based metal matrix composites. Int Mater Rev 1997;41:41–58.
[5] Çam G, Koçak M. Progress in joining of advanced materials. Int Mater Rev 1998;43:1–39.
[6] Guo J, Gougeon P, Chen X-G. Study on laser welding of AA1100-16 vol.% B_4C metal-matrix composites. Compos: Part B 2012;43:2400–8.
[7] Thomas WM, Nicholas ED, Needham JC, Murch MG, Templesmith P, Dawes CJ. Friction-stir butt welding. G.B. Patent 9125978.8, UK: 1991.
[8] Mishra RS, Ma ZY. Friction stir welding and processing. Mater Sci Eng R 2005;50:1–78.
[9] Threadgill PL, Leonard AJ, Shercliff HR, Withers PJ. Friction stir welding of aluminium alloys. Int Mater Rev 2009;54:49–93.
[10] Chen T. Process parameters study on FSW joint of dissimilar metals for aluminum-steel. J Mater Sci 2009;44:2573–80.
[11] Mofid MA, Abdollah-zadeh A, Ghaini FM. The effect of water cooling during dissimilar friction stir welding of Al alloy to Mg alloy. Mater Des 2012;36:161–7.
[12] Sato YS, Park SHC, Michiuchi M, Kokawa H. Constitutional liquation during dissimilar friction stir welding of Al and Mg alloys. Scripta Mater 2004;50:1233–6.
[13] Sharifitabar M, Nami H. Microstructures of dissimilar friction stir welded joints between 2024-T4 aluminium alloy and Al/Mg_2Si metal matrix cast composite. Compos: Part B 2001;42:2004–12.
[14] Pan C, Hu L, Li Z, North TH. Microstructural features of dissimilar MMC/AISI 304 stainless steel friction joints. J Mater Sci 1996;31:3667–74.
[15] Rodrigues DM, Loureiro A, Leitao C, Leal RM, Chaparro BM, Vilaça P. Influence of friction stir welding parameters on the microstructural and mechanical properties of AA 6016-T4 thin welds. Mater Des 2009;30:1913–21.
[16] Kumar K, Kailas SV. Positional dependence of material flow in friction stir welding: analysis of joint line remnant and its relevance to dissimilar metal welding. Sci Technol Weld Joining 2010;15:305–11.
[17] Steuwer A, Peel MJ, Withers PJ. Dissimilar friction stir welds in AA5083–AA6082: the effect of process parameters on residual stress. Mater Sci Eng A 2006;441:187–96.
[18] Silva AAMd, Arruti E, Janeiro G, Aldanondo E, Alvarez P, Echeverria A. Material flow and mechanical behaviour of dissimilar AA2024-T3 and AA7075-T6 aluminium alloys friction stir welds. Mater Des 2011;32:2021–7.
[19] Jun T-S, Dragnevski K, Korsunsky AM. Microstructure, residual strain, and eigenstrain analysis of dissimilar friction stir welds. Mater Des 2010;31:S121–5.
[20] Sundaram NS, Murugan N. Tensile behavior of dissimilar friction stir welded joints of aluminium alloys. Mater Des 2010;31:4184–93.
[21] Nandan R, DebRoy T, Bhadeshia HKDH. Recent advances in friction-stir welding – process, weldment structure and properties. Prog Mater Sci 2008;53:980–1023.
[22] Park S-K, Hong S-T, Park J-H, Park K-Y, Kwon Y-J, Son H-J. Effect of material locations on properties of friction stir welding joints of dissimilar aluminium alloys. Sci Technol Weld Joining 2010;15:331–6.
[23] Aval HJ, Serajzadeh S, Kokabi AH. Thermo-mechanical and microstructural issues in dissimilar friction stir welding of AA5086–AA6061. J Mater Sci 2011;46:3258–68.
[24] Lee WB, Yeon YM, Jung SB. The mechanical properties related to the dominant microstructure in the weld zone of dissimilar formed Al alloy joints by friction stir welding. J Mater Sci 2003;38:4183–91.
[25] Srinivasan PB, Dietzel W, Zettler R, Santos JFd, Sivan V. Effects of inhibitors on corrosion behaviour of dissimilar aluminium alloy friction stir weldment. Corros Eng Sci Technol 2007;42:161–7.
[26] ASM Handbook Committee. Properties and selection: nonferrous alloys and special-purpose materials. Materials Park, OH: ASM International; 1991.
[27] Sato YS, Kokawa H, Enomoto M, Jogan S. Microstructural evolution of 6063 aluminium during friction-stir welding. Metall Mater Trans A 1999;30:2429–37.
[28] Frigaard Ø, Grong Ø, Midling OT. A process model for friction stir welding of age hardening aluminum alloys. Metall Mater Trans A 2001;32A:1189–200.
[29] Riahi M, Nazari H. Analysis of transient temperature and residual thermal stresses in friction stir welding of aluminum alloy 6061-T6 via numerical simulation. Int J Adv Manuf Technol 2011:143–52.
[30] Akeret R. Extrusion of semifinished products in aluminum alloys. In: Bauser M, Sauer G, Siegert K, editors. Extrusion. Materials Park, OH 44073-0002: ASM International; 2006. p. 207–26.
[31] Amancio-Filho ST, Sheikhi S, Santos JFD, Bolfarini C. Preliminary study on the microstructure and mechanical properties of dissimilar friction stir welds in aircraft aluminium alloys 2024-T351 and 6056-T4. J Mater Process Technol 2008;206:132–42.
[32] Hutchinson B. Nucleation of recrystallization. Scr Metall Mater 1992;27:1471–5.
[33] McNelley TR, Swaminathan S, Su JQ. Recrystallization mechanisms during friction stir welding/processing of aluminum alloys. Scripta Mater 2008;58:349–54.
[34] Humphreys FJ. Local lattice rotations at 2nd phase particle in deformed metals. Acta Mater 1979;27:1801–14.
[35] Humphreys FJ, Hatherly M. Recrystallization and related annealing phenomena. 2nd ed. Elsevier Ltd.; 2004.
[36] Hassan KhAA, Norman AF, Price DA, Prangnell PB. Stability of nugget zone grain structures in high strength Al alloy friction stir welds during solution treatment. Acta Mater 2003;51:1923–36.
[37] Su J-Q, Nelson TW, Mishra R, Mahoney M. Microstructural investigation of friction stir welded 7050-T651 aluminium. Acta Mater 2003;51:713–29.
[38] ASM Handbook Committee. Heat treating. Materials Park, OH: ASM International; 1991.
[39] Koilraj M, Sundareswaran V, Vijayan S, Rao SRK. Friction stir welding of dissimilar aluminum alloys AA2219 to AA5083 – Optimization of process parameters using Taguchi technique. Mater Des 2012;42:1–7.
[40] AWS D17 Committee on Welding in the Aircraft and Aerospace Industries. Specification for friction stir welding of aluminum alloys for aerospace hardware. Miami, Florida: American Welding Society; 2010. p. 60.
[41] Kerlins V. Modes of fracture. In: ASM Handbook Committee Editors. Fractography. Materials Park, OH: ASM, International; 1991.